

REL-SF4PASS: Panoramic Semantic Segmentation with REL Depth Representation and Spherical Fusion

Xuewei Li¹, Xinghan Bao¹, Zhimin Chen¹, Xi Li^{2*}

¹School of Electronic and Information Engineering, Shanghai DianJi University

²College of Computer Science and Technology, Zhejiang University

Abstract

As an important and challenging problem in computer vision, Panoramic Semantic Segmentation (PASS) aims to give complete scene perception based on an ultra-wide angle of view. Most PASS methods often focus on spherical geometry with RGB input or using the depth information in original or HHA format, which does not make full use of panoramic image geometry. To address these shortcomings, we propose **REL-SF4PASS** with our **REL** depth representation based on cylindrical coordinate and Spherical-dynamic Multi-Modal Fusion (SMMF). **REL** is made up of **R**ectified Depth, **E**levation-Gained Vertical Inclination Angle, and **L**ateral Orientation Angle, which fully represents 3D space in cylindrical coordinate style and the surface normal direction. SMMF aims to ensure the diversity of fusion for different panoramic image regions and reduce the breakage of cylinder side surface expansion in ERP projection, which uses different fusion strategies to match the different regions in panoramic images. Experimental results show that **REL-SF4PASS** considerably improves performance and robustness on popular benchmark, Stanford2D3D Panoramic datasets. It gains 2.35% average mIoU improvement on all 3 folds and reduces the performance variance by approximately 70% when facing 3D disturbance.

1. Introduction

There has been a great growing trend of practical applications based on 360° cameras in recent years, including holistic sensing in autonomous vehicles [6, 11, 21], immersive viewing in augmented reality and virtual reality devices [1, 29, 30, 39], etc. Panoramic images with a complete Field of View (FoV, which is 360° × 180°) deliver complete scene perception in many real-world scenarios, thus drawing increasing attention in the research community in computer vision. Panoramic semantic segmentation (PASS) is essential for omnidirectional scene understanding, as it

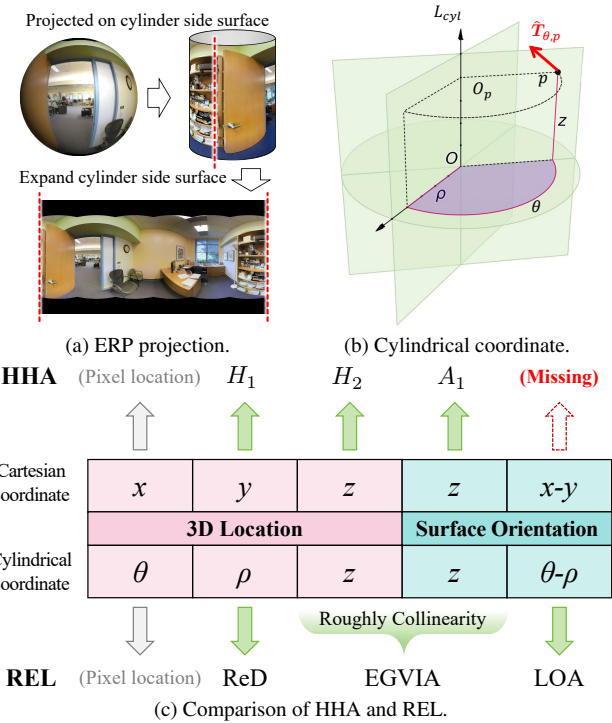


Figure 1. Overview of ERP projection, cylindrical coordinate and comparison of HHA and REL. $\hat{T}_{\theta,p}$ is the tangent line to circle O_p at point p . Circle O_p lies in the plane perpendicular to gravity, passes through point p , and its center lies on the cylindrical axis L_{cyl} of $\rho\theta z$. In (c), we compared how different structure information are represented in REL and HHA.

gives pixel-wise analysis for panoramic images and offers a dense prediction technical route acquiring complete perception of surrounding scenes [33]. Most existing PASS approaches use equirectangular projection (ERP) [10, 25, 34] to convert original 360° data to 2D panoramic images. In brief, the original spherical information is first projected onto the side surface of a cylinder, and then the cylinder side surface is expanded as shown in Fig. 1a.

Compared with RGB-only input, PASS strategies with

RGB and depth input gain better performance, because depth information D includes 3D location and shape (typically represented by surface normal) of each pixel beneficial to dense prediction like PASS. HHA [13] is widely used to explicitly model the 3D location and surface normal of each pixel in camera cartesian coordinate with horizontal disparity (first H , H_1), height above ground (second H , H_2), and the angle between surface normal and gravity direction (last A , A_1), which gain considerable improvement compared with directly using original D . 3D location has 3 degrees of freedom when surface normal direction has 2 degrees of freedom. As shown in Fig. 1c, HHA representation utilizes 3 different channels (H_1 , H_2 , and A_1) and the pixel location in the image to represent 4 degrees of freedom information. However, the representation of the second degree of freedom for the surface normal direction is missing. Furthermore, the HHA calculation depends on the camera posture and intrinsics (e.g., the focal length), which is not comfortable enough to deal with image-only data.

Facing this limitation and inspired by the cylinder used in ERP, we propose REL representation and directly use cylindrical coordinate $\rho\theta z$ to represent the 3D location and surface normal of each pixel. REL representation is composed of Rectified Depth (ReD), Elevation-Gained Vertical Inclination Angle (EGVIA), and Lateral Orientation Angle (LOA). Firstly, as shown in Fig. 1c, for the point p in 3D space that corresponds to a certain pixel, we calculate the plane distance ρ , the plane angle θ , and the height z (the same as H_2) to directly represent the 3D location. Secondly, we calculate the angle between surface normal and gravity direction and lateral orientation angle which is the angle between surface normal and tangent line $\hat{T}_{\theta,p}$. Also, REL representation does not need camera posture and intrinsics. Furthermore, we find roughly collinearity between H_2 and A_1 in panoramic images (discussed in Fig. 5 in detail), we fuse H_2 and A_1 as our EGVIA, set planar distance ρ as our ReD, use lateral orientation angle as LOA, and gain our REL representation. It has 3 channels and is the same as HHA for a relatively fair comparison.

In addition, due to the different local situations (e.g., distortion, location, etc.) of different regions in the panoramic image caused by ERP, we propose our Spherical-dynamic Multi-Modal Fusion (SMMF) to effectively fuse the RGB and REL information for different regions of panoramic images by different ways. Instead of achieving regions from input images, SMMF uses overlapping regions sampled on the cylinder side surface to reduce the breakage to the scene structure caused by cylinder side surface expansion. It not only allows different fusion ways for different regions, but also extracts semantic features across the left and right edges of a panoramic images. Using REL representation and SMMF jointly, we build up REL-SF4PASS, and our contributions are summarized as follows:

- We propose our 3-channel REL representation to represent the 3D location and shape of each pixel based on cylindrical coordinate.
- Our Spherical-dynamic Multi-Modal Fusion (SMMF) enriches the diversity of fusion for different regions in panoramic images and reduce the impact of cylinder side surface expansion by ERP projection.
- We evaluate REL-SF4PASS on popular Stanford2D3D Panoramic datasets, and gain the 2.35% average mIoU improvement on all 3 folds. Also, it reduces the performance variance by about 70% in SGA validation.

2. Related Work

The two most related fields are panoramic semantic segmentation and RGB-D semantic segmentation.

2.1. Panoramic Semantic Segmentation

PAnoramic Semantic Segmentation (PASS) is the task that does semantic segmentation on panoramic images. In recent years, many models have been developed for PASS. Deng et al. [7] built up the first semantic segmentation framework for big FoV (wide-angle / fish-eye) images. Furthermore, Yang et al. [32] used attention connections to make PASS more efficient, and DS-PASS was proposed. Common PASS solutions can be divided into two main fields: geometry-aware strategies and distortion-aware ones. For geometry-aware strategies [18–20, 23], some utilized 2D geometry like horizontal features mainly based on the ERP inherent property when some use 3D geometry. Tateno et al. [26] used carefully designed distortion-aware convolutions to deal with image distortions when Jiang et al. [16] utilized a spherical convolution operation. SliceNet [23] and HoHoNet [25] used 1D horizontal representation to construct their feature maps. ACD-Net [41] proposed convolution equipped with different dilation rates adaptively in PASS. Trans4PASS [35] and Trans4PASS+ [37] proposed their Deformable Patch Embedding (DPE) and Deformable Multi-Layer Perception (DMLP) modules to perceive and deal with spherical distortion. SGAT4PASS [18] designed a reprojection strategy to augment training samples and used SDPE to apply the spherical symmetry into the deformable components in the model. For distortion-aware strategies, Lee et al. [17] represented panoramic views with spherical polyhedrons to minimize the difference in spatial resolution of the surface of the sphere. Liu et al. [20] proposed their spherical discrete sampling based on the weights of the pre-trained models in order to mitigate distortions effectively.

2.2. RGB-D Semantic Segmentation

RGB-D semantic segmentation takes advantage of both RGB and depth information and gets considerable performance improvements. Previous works mainly focus on two

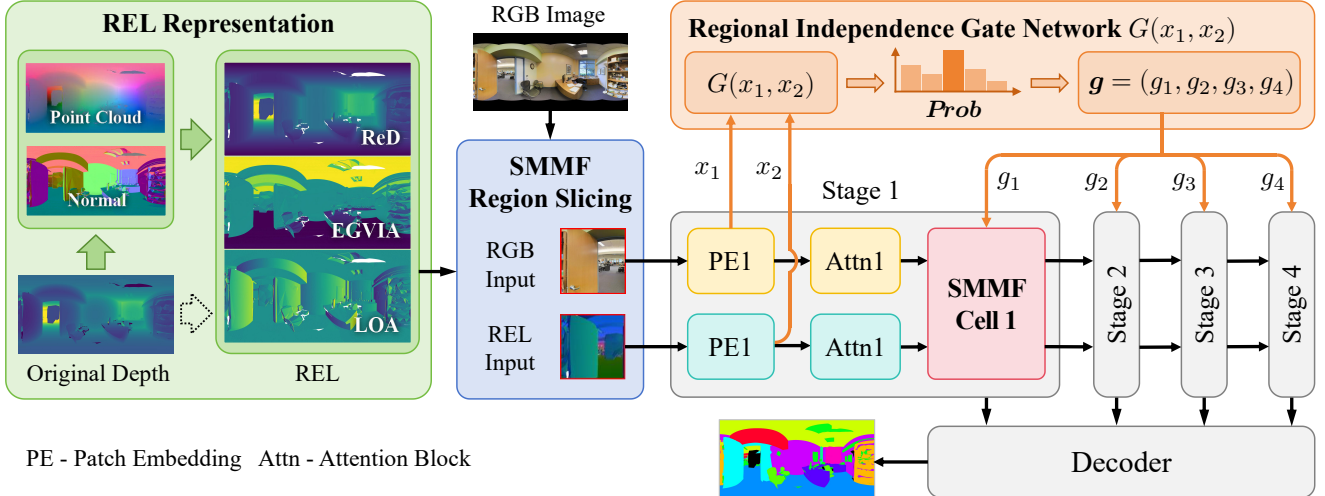


Figure 2. The overview of REL-SF4PASS. Firstly, REL representation effectively represents the depth information by using ReD, EGVIA, and LOA, which contains the 3D location and surface normal direction. Secondly, Our SMMF to get image regions from cylinder side surface and uses a Gate Network to independently determine the fusion used in each region.

aspects: (a) new operators / layers / modules based on the geometric properties of RGB-D data [4, 5, 15, 27, 28]; (b) making specialized architectures for jointly utilizing RGB and depth features [14, 22, 25, 36, 38]. For the former ones, models are carefully designed. E.g., ACNet [15] gained informative features from RGB-D data by attention. For the latter one, various RGB and depth information fusion ways have been explored. E.g., CMX [36] built CM-FRM to use one modality features to rectify the features of the other one, and proposed FFM to make enough long-range context interaction.

REL-SF4PASS focuses on RGB-D PASS task, we carefully design our REL representation for the geometric structure of panoramic images, and our SMMF as a spherical-guided region-adaptive dynamic multi-modal fusion.

3. Method

REL-SF4PASS is introduced in this section. First, we introduce the background, notations, and classic HHA in Section 3.1. Second, we propose our REL representation made up of Rectified Depth, Elevation-Gained Vertical Inclination Angle, and Lateral Orientation Angle. Furthermore, our Spherical-dynamic Multi-Modal Fusion (SMMF) utilizes depth information more efficiently and is introduced in Section 3.3. The overall pipeline is shown in Fig. 2.

3.1. Background and Notations

We first describe the common formulation of panoramic images and classic HHA. For expression convenience, we build up several coordinates:

- 1) Image coordinate uvd (u : pixel column (positive

to the right), v : pixel row (positive downward), d : Pixel depth), and the origin is image upper left corner;

2) Gravity-correction camera cartesian coordinate xyz (right-handed): using camera as origin, first define y positive direction as from camera to target pixel, and then gravity correction is performed with rectifying the direction of gravity as the negative z direction.

3) Spherical coordinate $r\theta\phi$ (r is the radius, θ is the azimuth / longitude (from -180° to 180°), ϕ is the elevation / latitude (from -90° to 90°), and the origin is the camera).

ERP projection is widely-used to transform original 360° data into 2D panoramic images. As shown in Fig. 1a, 360° data is first projected onto the cylinder side surface and then expand the cylinder side surface. Original 360° data is formulated in the spherical coordinate. To convert it to a rectangular image in the image coordinate, let $u = (\theta - \theta_0)\cos\phi_1$ and $v = (\phi - \phi_1)$. $\theta_0 = 0$ is the central latitude and $\phi_1 = 0$ is the central longitude. The ERP-processed rectangular images are the input in PASS, and the rectangular semantic segmentation results are the final output to calculate metrics.

HHA representation changes original depth information D to 3 channels with the help of camera intrinsics: horizontal disparity (first H , H_1), height above ground (second H , H_2), and the angle between surface normal and gravity direction (last A , A_1). It is calculated as (all values are linearly scaled to $[0, 255]$): (1) Calculate H_1 from the original depth information D and camera intrinsics (see Section A “Details for Constructing 3D Point Cloud” in the supplementary material); (2) Convert D to a 3D point cloud with camera intrinsics, gain the normal field, estimate gravity direction, calculate the gravity-corrected 3D point cloud P

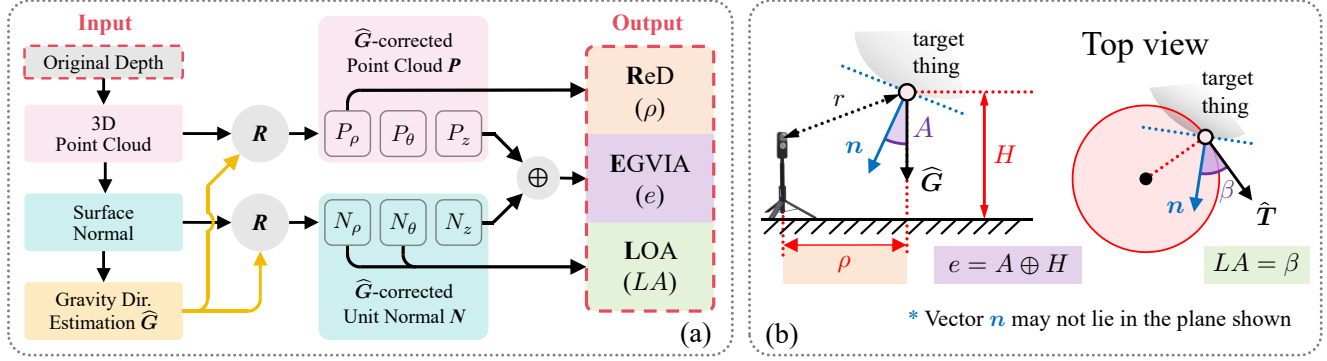


Figure 3. The calculation process (a) and physical model (b) of REL representation. In (a), \mathbf{R} is 3D Rigid Body Rotation, and \oplus is Eq. (4).

and normal field N . (3) Calculate H_2 and A_1 using [12].

As shown in Fig. 1c, the representation of the second degree of freedom for the surface normal direction is missing.

3.2. REL Representation

Dealing with the limitation above, we make full use of the geometry of panoramic images to design our REL directly represent the 3D location and surface normal of each pixel based on cylindrical coordinate $\rho\theta z$.

Firstly, compared with plane images, panoramic images provide a complete FoV and carry rich prior information, such as using pixel location in image coordinate can derive the direction of corresponding point from camera without using camera intrinsics (see Section A “Details for Constructing 3D Point Cloud” in the supplementary material).

Secondly, for a certain point p , its location in gravity-correction camera cartesian coordinate is (p_x, p_y, p_z) and its unit surface normal is (N_x^p, N_y^p, N_z^p) . Our REL representation model the position in 3D space by planar distance, plane angle and height based on cylindrical coordinate $\rho\theta z$, and model unit normal N with 2 independent angle, the angle between surface normal and gravity direction and the angle between surface normal and planar tangent line $\hat{T}_{\theta,p}$. Our Rectified Depth (ReD) ρ_p corresponds to the planar distance. The plane angle θ can be directly gained by pixel spherical coordinate $r\theta\phi$ representation. Our Elevation-Gained Vertical Inclination Angle (EGVIA) e_p integrates 2 roughly collinearity components, height H_p and the angle between surface normal and gravity direction (indicating N_z^p) with normalization. Our Lateral Orientation Angle (LOA) indicates the angle between surface normal and planar tangent line $\hat{T}_{\theta,p}$. For N is unit vector with 2 degrees of freedom, 2 angles are enough. The physical models of all 3 above are shown in the right part of Fig. 3.

In calculation, as shown in the left part of Fig. 3, REL only needs original depth image input (without camera posture or intrinsics) to gain gravity-corrected 3D point cloud P and achieve the normal field N , and all channels are cal-

culated based on P and N .

3.2.1. Rectified Depth

Rectified depth ρ_p aims to represent the planar distance between camera and p , so it is defined as:

$$\rho_p = \sqrt{p_x^2 + p_y^2} = d_p \cos \phi_p, \quad (1)$$

where d_p is the depth distance of p , and ϕ_p is gained from the input image and gravity correction.

3.2.2. Elevation-Gained Vertical Inclination Angle

To calculate elevation-gained vertical inclination angle of p , we should first gain the height H_p (the same definition as H_2 in HHA) and the angle between surface normal and gravity direction A_p (the same as A_1 in HHA) of p . we calculate the height H_p as:

$$H_p = p_z - \min\{P_z\}, \quad (2)$$

where $\min\{P_z\}$ means the minimum value of p_z among all p in P . We calculate A_p as:

$$A_p = \arccos(N^p \odot \hat{\mathbf{G}}) = \arccos N_z^p, \quad (3)$$

where \odot is dot product, N^p is the surface normal of p , $\hat{\mathbf{G}}$ is the unit vector of the gravity direction that is $(0, 0, -1)$ in xyz , and N_z^p is the z-axis component of N^p .

For panoramic images with complete FoV, the change of camera direction does not affect the whole imaging content when its representation is mainly influenced by ERP projection. For humans, ERP projection has a popular and conventional usage, that is, the normal vector of bottom plane in the cylinder used for ERP projection is parallel to the direction of gravity. As a result, for panoramic images with common ERP projection, it is most the ground when ϕ is close to -90° and it is most the sky or ceiling when ϕ is close to 90° , which makes normalized H_p and A_p highly related. Fig. 5 is a visualization. The main difference between H_p and A_p is: (1) For nearly horizontal surface (such

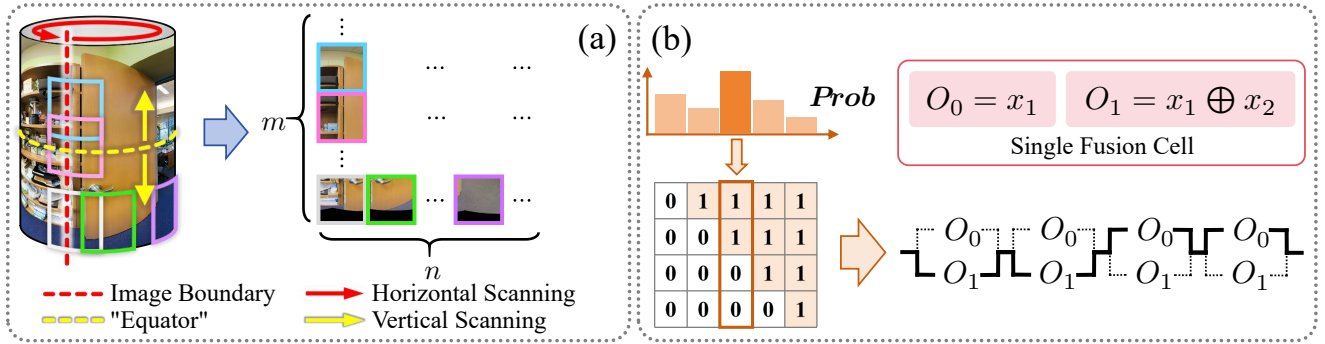


Figure 4. The detail design of SMMF Region Slicing (a) and Gate Network (b). Slicings have overlap and \oplus means the fusion operation.

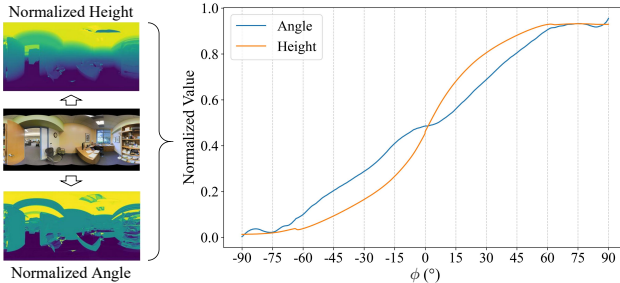


Figure 5. Comparison of normalized height and the angle between surface normal and gravity direction (short as Angle). The x-axis of the right figure is ϕ (from -90° to 90°) when the y one is the average of all normalized corresponding values.

as ground, tabletop, etc.), H_p can distinguish different surface more directly than A_p ; (2) For nearly vertical surface (such as wall, etc.), whose A_p are close to 90° . Based on these observations and to represent this information more efficiently, we propose elevation-gained vertical inclination angle \hat{e}_p of a certain point p as:

$$\hat{e}_p = \begin{cases} \lambda \hat{A}_p + (1 - \lambda) \hat{H}_p, & A_p \in [0^\circ, \alpha) \cup (180^\circ - \alpha, 180^\circ], \\ \hat{A}_p, & A_p \in [\alpha, 180^\circ - \alpha] \end{cases} \quad (4)$$

where \hat{A}_p and \hat{H}_p are normalized A_p and H_p (linearly scaled to $[0, 255]$ [12]). Using elevation-gained vertical inclination angle \hat{E}_p , we jointly represent height and the angle between surface normal and gravity direction.

3.2.3. Lateral Orientation Angle

The rest component is the angle between surface normal and planar tangent line $\hat{T}_{\theta,p}$. In detail, $\hat{T}_{\theta,p}$ is the tangent line to circle O_p at point p , where circle O_p lies in the plane perpendicular to the direction of gravity, its center lies on the cylindrical axis L_{cyl} of $\rho\theta z$, and passes through point p . we define our lateral orientation angle LA_p to represent it

of p as:

$$\hat{L}A_p = \text{Norm}(\arccos(N^p \odot \hat{\mathbf{T}})) \quad (5)$$

$$= \text{Norm}(\arccos(N_x^p \cdot \cos \theta + N_y^p \cdot \sin \theta)), \quad (6)$$

where \odot is dot product, $\hat{\mathbf{T}}$ is the unit vector of tangent to the latitude that p belongs to, $(\cos \theta, \sin \theta, 0)$, and N_x^p / N_y^p is the x-axis / y-axis component of N^p . $\text{Norm}(\cdot)$ is the normalization for linearly scaled to $[0, 255]$ [12].

3.3. Spherical-dynamic Multi-Modal Fusion

After using REL to represent depth information, we need to fuse it and RGB information effectively. A common way is to fuse the two information after each block in the model but lacks diversity. Sample-adaptive fusion [31], is classic but effective way for this problem. For panoramic images based on ERP projection, there is some structural prior. E.g., the pixels have the same latitude in the spherical coordinate so that their distortion and semantics are somehow similar. For example, the upper part (Latitude ϕ is close to 90°) of an indoor panoramic image is mostly the ceiling, the lower one (Latitude ϕ is close to -90°) is mostly the floor, and the middle one (Latitude ϕ is close to 0°) usually has richer semantics. It is necessary to adopt different fusion strategies for different latitude regions, that is, to refine the adaptive granularity of fusion from the sample level to the regional level. Also, the cylinder side surface expansion in ERP projection breaks the scene structure in panoramic images.

Inspired by DynMM [31] and faced with 2 challenges above, we propose our Spherical-dynamic Multi-Modal Fusion (SMMF), which uses different fusion strategies for not only different inference images but also different regions in one image. Instead of achieving regions from panoramic images, SMMF uses overlapping regions directly sampled on the cylinder side surface to reduce the breakage to the scene structure caused by cylinder side surface expansion. As shown in the left part of Fig. 4, we sample $m \times n$ (m rows and n columns) overlap regions on the cylinder side surface. In the horizontal direction, we allow the regions

Method	modal	Avg mIoU	F1 mIoU
StdConv (2018) [26]	RGB	-	32.6
CubeMap (2018) [26]	RGB	-	33.8
DistConv (2018) [26]	RGB	-	34.6
SWSCNN (2020) [9]	RGB	43.4	-
Tangent (2020) [8]	RGB	45.6	-
HoHoNet (2021) [25]	RGB	52.0	53.9
PanoFormer (2022) [24]	RGB	48.9	-
Trans4PASS (2022) [35]	RGB	52.1	53.3
FreDSNet (2023) [3]	RGB	-	46.1
CBFC (2023) [40]	RGB	52.2	-
SGTA4PASS (2023) [18]	RGB	55.3	56.4
Trans4PASS+ (2024) [37]	RGB	53.7	53.6
Twin (2025) [19]	RGB	55.85	-
Tangent (2020) [8]	RGB-D	52.50	-
HoHoNet (2021) [25]	RGB-D	56.73	-
PanoFormer (2022) [24]	RGB-D	57.03	-
CBFC (2023) [40]	RGB-D	56.70	-
SFSS (2024) [14]	RGB-D	55.49	-
SFSS (2024) [14]	RGB-N	59.43	-
SFSS (2024) [14]	RGB-HHA-D	59.99	-
SFSS (2024) [14]	RGB-HHA-N	60.24	-
SFSS (2024) [14]	RGB-HHA	60.60	-
CMX* [36]	RGB-HHA	60.71	63.98
Ours	RGB-REL	63.06	67.37

Table 1. Comparison with the SOTA methods on Stanford2D3D Panoramic datasets with traditional metrics. We follow recent works to compare the performance of both official fold 1 and the average performance of all three official folds, respectively. “Avg mIoU” / “F1 mIoU” means the mIoU performance of three official folds on average / official fold 1. The performance from StdConv (2018) to Trans4PASS+ (2024) are directly cited from [18]. Following, the performance from Twin (2025) to SFSS (2024) with RGB-D are directly cited from [19] and no fold 1 mIoU is provided. SFSS (2024) [14] from RGB-N to RGB-HHA are directly cited from [14] and “-N” means using normals modalities. CMX* is our implementation for CMX [36] on this PASS task. Considerable improvement is gained and our REL representation is more suitable for model training.

selecting across the left and right edges of the panoramic image to reduce the influence of cylindrical side surface expansion in ERP projection. In the vertical direction, different from common image region generation [31], we start from the “equator” ($\phi = 0^\circ$) and proceed sequentially towards the top and bottom edges of the image to ensure the obtained regions symmetrical about the equator. (E.g., begin from the pick square to the blue / gray square in the left part of Fig. 4) We take into account all related region fusion modes for the overlap area, and sum them as the final result.

For the detailed RGB-D fusion design, we insert several fusion cell $FusCell_i$ to fuse 2 modalities, $M = \{M_{RGB}, M_D\}$. As widely-used Mixture-of-Experts (MoE) ways, for the fusion cell $FusCell_i$ in stage i , we make a set of B expert fusion operations in parallel as $\{FusOp_i\}$, which specializes in a subset of two modalities. In particular, M_D includes scene structure cues but often performs poorly by themselves in semantic segmentation without RGB input, so that M_D is not used alone. A gate network $G(x)$ is designed to decide which expert network should be activated. It produces a B -dimensional vector

$\mathbf{Prob} = [Prob_1, Prob_2, \dots, Prob_B]$ for each $FusCell_i$. The output $OutCell_i$ of cell $FusCell_i$ is $OutCell_i = \sum_{i=1}^B Prob_i \cdot FusOp_i(x)$ with multi-modal input as shown in the right part of Fig. 4. Similar to DynMM [31], we use two-stage soft-hard training and early stop. The whole training is divided into two stages: soft training and hard training. For soft training stage, \mathbf{Prob} is a “soft” probability vector whose each value may be non-zero when \mathbf{Prob} must be one-hot in hard training stage. we set 0 means no fusion (using RGB only) and 1 means using RGB-D fusion for convenience. For fusion early stop, it means that if 0 (no fusion) is selected in a previous cell $FusCell_i$, all the following cells $FusCell_j$, ($j > i$) are forced to 0.

Using REL representation and SMMF jointly, we clearly represent depth information and use a spherical adaptive method to effectively fuse multi-modal information.

4. Experiments

4.1. Datasets and Protocols

We validate REL-SF4PASS on Stanford2D3D Panoramic datasets [2]. It has 1413 panoramic images with 13 labeled semantic classes. It has 3 official folds, fold 1, fold 2, and fold 3. We follow previous works [18, 35, 37] setting.

Our experiments were conducted with a server with 8 NVIDIA GeForce RTX 3090 GPUs. We use CMX [36] as our baseline and the height / width of input images are 2048 / 4096 pixels, and set $\alpha/\lambda/m/n = 45^\circ/0.5/3/7$. Each region is 1080×1080 , and the region stride is 720 pixels at inference. We overall follow [31] for training and set soft / hard training epochs is both 100, and T decays from 1 to 0.1 in the 100 soft training epochs.

SGA validation Most PASS datasets follow a unified ERP way to deal with original 360° data so that whether PASS models have the potential to overfit the ERP pattern is questionable. It may have poor 3D robustness so that SGA validation [18] is also used in validation. In detail, “Mean” means the average of all results (e.g., mIoU, per pixel accuracy, etc.). For a general rotation in a 3D space, the angles of yaw / pitch / roll are $\alpha/\beta/\gamma$. Similar to [18], we set 3D rotation disturbance is at most $5^\circ/5^\circ/360^\circ$ of $\beta/\gamma/\alpha$. We set $n_\alpha = 4$ ($0^\circ, 90^\circ, 180^\circ, 270^\circ$), $n_\beta = 2$ ($0^\circ, 5^\circ$), and $n_\gamma = 2$ ($0^\circ, 5^\circ$). “Variance” means the variance of all results. “Range” means the gap between the maximum and minimum results. Compared to traditional one, SGA validation avoids models gaining performance by fitting the datasets ERP pattern and reflects objective 3D robustness.

4.2. Performance Comparison

We first compare with several recent SOTA methods with traditional metrics. Also, we compare REL-SF4PASS with the baseline using HHA and SGAT4PASS [18] in detail with SGA metrics to validate 3D robustness.

(β, γ, α) ($^{\circ}$)	HHA mIoU / PAcc		(β, γ, α) ($^{\circ}$)	HHA mIoU / PAcc		(β, γ, α) ($^{\circ}$)	HHA mIoU / PAcc	
	Our mIoU	PAcc		Our mIoU	PAcc		Our mIoU	PAcc
(0,0,0)	65.433	/ 90.786	(0,5,0)	61.877	/ 88.571	(5,0,0)	61.252	/ 88.310
	67.367	/ 90.912		65.391	/ 89.846		65.251	/ 89.730
(0,0,90)	65.597	/ 90.745	(0,5,90)	61.525	/ 88.371	(5,0,90)	62.515	/ 88.880
	67.010	/ 90.834		65.138	/ 89.755		65.285	/ 89.799
(0,0,180)	65.507	/ 90.764	(0,5,180)	62.363	/ 88.924	(5,0,180)	61.742	/ 88.363
	67.223	/ 90.891		65.490	/ 89.848		65.475	/ 89.959
(0,0,270)	65.852	/ 90.782	(0,5,270)	62.050	/ 88.453	(5,0,270)	62.503	/ 88.596
	67.145	/ 90.904		65.179	/ 89.877		65.019	/ 89.780

Table 2. Detail performance comparison of REL and HHA both with SMMF on Stanford2D3D Panoramic datasets fold 1 with SGA metrics. All 16 test situations are shown, and the analysis is in Tab. 3. “PAcc” meas the pixel accuracy metric.

Statistics	HHA				REL-SF4PASS			
	mIoU	PAcc	mIoU	PAcc	mIoU	PAcc	mIoU	PAcc
Mean	62.237	88.766	65.380	(+3.143)	89.891	(+1.126)		
Variance	5.316	1.801	1.607	(-3.709)	0.472	(-1.328)		
Range	6.722	3.810	3.974	(-2.748)	2.062	(-1.748)		

Table 3. Overall performance comparison with HHA with Fold 1 on Stanford2D3D Panoramic datasets based on Tab. 2. “PAcc” means the pixel accuracy metric. REL representation earns considerable mean performance and robustness improvement.

Statistics	SGAT4PASS		OmniREL-Reproj		
	mIoU	PAcc	mIoU	PAcc	
Mean	55.984	82.887	65.040	(+9.056)	
Variance	0.066	0.020	0.021	(-0.045)	
Range	0.940	0.478	0.544	(-0.397)	
				0.174	(-0.304)

Table 4. Overall SGA validation performance comparison with SGAT4PASS [18] on Stanford2D3D Panoramic datasets. “PAcc” means the pixel accuracy. REL-SF4PASS earns significant mean performance and robustness improvement. For fair comparison, the SGA validation setting and data augmentation in training is the same as SGAT4PASS [18].

Traditional metrics. Comparison results on Stanford2D3D Panoramic datasets with SOTA methods are shown in Tab. 1. Following recent work, we report the performance of both official fold 1 and the average performance of all three official folds. A considerable improvement of 2.35% / 3.39% on the mIoU performance of 3 official folds on average / official fold 1 is observed and our REL representation is more suitable for model training.

SGA metrics. Comparison results with HHA on Stanford2D3D Panoramic datasets in SGA validation [18] are shown in Tab. 3. Tab. 2 is the detailed performance of each

D Info.	mIoU
RGB	51.25
RGB-D	59.03
RGB-ReD	62.02
RGB-EGVIA	63.35
RGB-Angle	59.76
RGB-Height	62.47
RGB-LOA	61.28
RGB-REL	64.47
RGB-HHA-DyMM	64.59
RGB-REL-DyMM	66.73
RGB-HHA-SMMF	65.43
RGB-REL-SMMF	67.37

Table 5. The effect of each module on Stanford2D3D Panoramic datasets fold 1 with traditional metrics. The “RGB-X” means using both RGB and X channels. “-DyMM” / “-SMMF” means using [31] / SMMF. Note that Angle / Height is \hat{A}_p and \hat{H}_p .

situation. The models are the same as “RGB-HHA-SMMF” and “RGB-REL-SMMF” in Tab. 5. For mean mIoU / pixel accuracy, an improvement of more than 3.1% / 1.1% is achieved, respectively. Furthermore, our variance / fluctuation is about 30% / 60% of the HHA ones. These results show that REL representation have a much better robustness than HHA.

Also, we compare the SGA validation [18] with SGAT4PASS having good resistance to 3D disturbances in Tab. 4. For fair comparison, the SGA validation setting and data augmentation in training are the same as SGAT4PASS [18]. Note that it is not the same as in Table 1, Table 3, and Table 2, which is optimized for SGA metrics instead of traditional metrics. For SGAT4PASS [18]

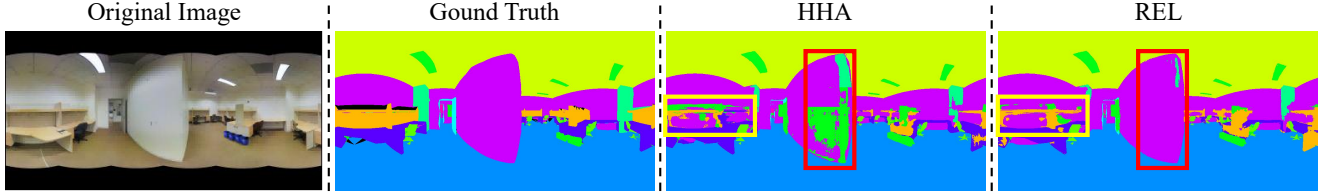


Figure 6. Comparison of HHA and REL results. Especially the region with changeable LOA, REL reduces the noise on wall in the red box when the details are clearer in the yellow box.

Probability of each strategy being selected in SMMF					
R1 C1	30.6	26.0	27.4	4.3	11.8
R1 C2	30.0	22.5	30.6	4.3	12.6
R1 C3	28.4	27.6	27.6	4.3	12.1
R1 C4	26.3	26.8	29.2	2.7	15.0
R1 C5	34.3	22.2	24.4	2.7	16.4
R1 C6	27.9	28.4	25.7	2.1	15.8
R1 C7	33.8	24.4	26.8	5.1	9.9
R2 C1	11.5	63.8	10.7	8.8	5.1
R2 C2	13.1	60.6	11.8	9.4	5.1
R2 C3	11.5	68.1	11.3	7.0	2.1
R2 C4	8.8	66.5	13.7	6.4	4.6
R2 C5	11.3	63.3	10.7	7.2	7.5
R2 C6	13.1	61.7	9.7	8.0	7.5
R2 C7	12.3	64.9	10.5	7.8	4.6
R3 C1	1.6	10.2	80.2	4.3	3.8
R3 C2	2.1	3.5	86.9	4.8	2.7
R3 C3	1.3	9.7	82.3	3.8	3.0
R3 C4	1.9	13.1	76.9	5.6	2.4
R3 C5	1.1	7.5	84.2	2.4	4.8
R3 C6	0.3	9.7	81.0	4.6	4.6
R3 C7	1.1	9.7	82.3	3.8	3.2

Figure 7. The visualization of the probability of each fusion strategy being selected for each region at inference. “RX CY” means the region in X^{th} row and Y^{th} column. The value is the probability (%) of choosing this fusion strategy throughout the inference process. a / b / c / d / e indicates $\mathbf{g} = [0, 0, 0, 0] / [1, 0, 0, 0] / [1, 1, 0, 0] / [1, 1, 1, 0] / [1, 1, 1, 1]$.

is RGB-based method, we mainly focus on variance and fluctuation. Our variance / fluctuation is also about 30% / 60% of the SGAT4PASS ones. The detailed performance is shown in Section B “The Detail Results Compared with SGAT4PASS” in the supplementary material.

4.3. Ablation Study

We discuss the contribution of REL representation and SMMF, the contribution of ReD, EGVIA, and LOA in REL representation, and the contribution of height and the angle between surface normal and gravity direction, in EGVIA.

Effect of REL Representation and SMMF The effectiveness of REL representation and SMMF is studied on Stanford2D3D Panoramic datasets official fold 1 with traditional metrics as shown in Table 5. Using our REL representation can improve RGB-D mIoU by 5.44%. Dynamic fusion benefit is considerable, and REL using DyMM gains 2.26% improvement when using our SMMF can further improve 0.64%. Similar performance improvements also appears on HHA.

Effect of Each Channel in REL The effectiveness of all

channels, ReD, EGVIA, and LOA, in REL representation are studied on Stanford2D3D Panoramic datasets official fold 1 with traditional metrics as shown in Table 5. Using ReD / EGVIA / LOA channel alone improves the RGB-D mIoU by 2.99% / 4.32% / 2.25%.

Effect of the different content of EGVIA The effectiveness of the height and the angle between surface normal and gravity direction, in EGVIA channel is studied on Stanford2D3D Panoramic datasets official fold 1 with traditional metrics as shown in Table 5. Using the angle between surface normal and gravity direction/ Height alone improves the RGB-D mIoU by 0.73% / 3.44%, when using a EGVIA improves the RGB-D mIoU by 4.32%.

4.4. Visualization

Visualization of different depth representation. We visualize the results of HHA and REL. Results show that REL reduces the noise and makes details clearer.

SMMF Spherical consistency. We visualize the strategy choice in SMMF to show whether REL-SF4PASS learns spherical geometry. It is easy to learn that due to different ERP patterns, the choice at the same latitude ϕ should be similar, or the different expansion for the cylinder side surface may lead to performance fluctuation. As shown in Fig. 7, it is the fusion strategy selections for all 21 regions at inference. We can learn that the regions in the same row (latitude) have a similar fusion strategy choice, indicating the spherical consistency.

More visualization are shown in Section C ‘More Visualizations’ in the supplementary material.

5. Conclusion

REL-SF4PASS is composed of a depth representation, REL representation, specifically for panoramic images and a region-level spherical-dynamic Multi-Modal Fusion to effectively integrate RGB and REL input. It applies spherical geometry prior to depth representation and fusion process, and shows considerable performance improvement and 3D robustness (e.g., resisting 3D disturbances) on popular datasets with both traditional and SGA metrics.

References

- [1] Hao Ai, Zidong Cao, Jinjing Zhu, Haotian Bai, Yucheng Chen, and Ling Wang. Deep learning for omnidirectional vision: A survey and new perspectives. *arXiv preprint arXiv:2205.10468*, 2022. 1
- [2] Iro Armeni, Sasha Sax, Amir R Zamir, and Silvio Savarese. Joint 2d-3d-semantic data for indoor scene understanding. *arXiv preprint arXiv:1702.01105*, 2017. 6
- [3] Bruno Berenguel-Baeta, Jesus Bermudez-Cameo, and Jose J Guerrero. Fredsnet: Joint monocular depth and semantic segmentation with fast fourier convolutions from single panoramas. In *Proc. ICRA*, pages 6080–6086. IEEE, 2023. 6
- [4] Jinming Cao, Hanchao Leng, Dani Lischinski, Daniel Cohen-Or, Changhe Tu, and Yangyan Li. Shapeconv: Shape-aware convolutional layer for indoor rgbd semantic segmentation. In *Proc. ICCV*, pages 7088–7097, 2021. 3
- [5] Lin-Zhuo Chen, Zheng Lin, Ziqin Wang, Yong-Liang Yang, and Ming-Ming Cheng. Spatial information guided convolution for real-time rgbd semantic segmentation. *IEEE Trans. Image Process.*, 30:2313–2324, 2021. 3
- [6] Greire Payen de La Garanderie, Amir Atapour Abarghouei, and Toby P Breckon. Eliminating the blind spot: Adapting 3d object detection and monocular depth estimation to 360 panoramic imagery. In *Proc. ECCV*, pages 789–807, 2018. 1
- [7] Liuyuan Deng, Ming Yang, Yeqiang Qian, Chunxiang Wang, and Bing Wang. Cnn based semantic segmentation for urban traffic scenes using fisheye camera. In *Proc. IEEE Intell. Vehicles Symp.*, pages 231–236. IEEE, 2017. 2
- [8] Marc Eder, Mykhailo Shvets, John Lim, and Jan-Michael Frahm. Tangent images for mitigating spherical distortion. In *Proc. CVPR*, 2020. 6
- [9] Carlos Esteves, Ameesh Makadia, and Kostas Daniilidis. Spin-weighted spherical cnns. *Proc. NeurIPS*, 33:8614–8625, 2020. 6
- [10] Zhiao Feng, Xuewei Li, Junjie Yang, Yuxin Peng, and Xi Li. Spheredrag: Spherical geometry-aware panoramic image editing. *arXiv preprint arXiv:2506.11863*, 2025. 1
- [11] Shaohua Gao, Kailun Yang, Hao Shi, Kaiwei Wang, and Jian Bai. Review on panoramic imaging and its applications in scene understanding. *arXiv preprint arXiv:2205.05570*, 2022. 1
- [12] Saurabh Gupta, Pablo Arbelaez, and Jitendra Malik. Perceptual organization and recognition of indoor scenes from rgbd images. In *Proc. CVPR*, pages 564–571, 2013. 4, 5
- [13] Saurabh Gupta, Ross Girshick, Pablo Arbeláez, and Jitendra Malik. Learning rich features from rgbd images for object detection and segmentation. In *Proc. ECCV*, pages 345–360. Springer, 2014. 2
- [14] Suresh Guttikonda and Jason Rambach. Single frame semantic segmentation using multi-modal spherical images. In *Proc. WACV*, pages 3222–3231, 2024. 3, 6
- [15] Xinxin Hu, Kailun Yang, Lei Fei, and Kaiwei Wang. Acnet: Attention based network to exploit complementary features for rgbd semantic segmentation. In *Proc. ICIP*, pages 1440–1444. IEEE, 2019. 3
- [16] Chiyu Jiang, Jingwei Huang, Karthik Kashinath, Philip Marcus, Matthias Niessner, et al. Spherical cnns on unstructured grids. *arXiv preprint arXiv:1901.02039*, 2019. 2
- [17] Yeonkun Lee, Jaeseok Jeong, Jongseob Yun, Wonjune Cho, and Kuk-Jin Yoon. Spheredph: Applying cnns on a spherical polyhedron representation of 360 degree images. *arXiv preprint arXiv:1811.08196*, 2018. 2
- [18] Xuewei Li, Tao Wu, Zhongang Qi, Gaoang Wang, Ying Shan, and Xi Li. Sgat4pass: spherical geometry-aware transformer for panoramic semantic segmentation. In *Proc. of IJCAI*, pages 1125–1133, 2023. 2, 6, 7
- [19] Jingguo Liu, Jiayao Liu, Yujie Wang, Shigang Li, and Jianfeng Li. A twin-network architecture for rgbd-based panoramic semantic segmentation. In *Proc. ICME Workshop*, pages 1–6. IEEE, 2025. 6
- [20] Jingguo Liu, Han Yu, Shigang Li, and Jianfeng Li. 360-degree full-view image segmentation by spherical convolution compatible with large-scale planar pre-trained models. In *Proc. ICME Workshop*, pages 1–6. IEEE, 2025. 2
- [21] Chaoxiang Ma, Jiaming Zhang, Kailun Yang, Alina Roitberg, and Rainer Stiefelhagen. Densepass: Dense panoramic semantic segmentation via unsupervised domain adaptation with attention-augmented context exchange. In *Proc. ITSC*, pages 2766–2772. IEEE, 2021. 1
- [22] Seong-Jin Park, Ki-Sang Hong, and Seungyong Lee. Rdfnet: Rgb-d multi-level residual feature fusion for indoor semantic segmentation. In *Proc. ICCV*, pages 4980–4989, 2017. 3
- [23] Giovanni Pintore, Marco Agus, Eva Almansa, Jens Schneider, and Enrico Gobbetti. Slicenet: deep dense depth estimation from a single indoor panorama using a slice-based representation. In *Proc. CVPR*, pages 11536–11545, 2021. 2
- [24] Zhijie Shen, Chunyu Lin, Kang Liao, Lang Nie, Zishuo Zheng, and Yao Zhao. Panoformer: panorama transformer for indoor 360° depth estimation. In *Proc. ECCV*, pages 195–211. Springer, 2022. 6
- [25] Cheng Sun, Min Sun, and Hwann-Tzong Chen. Hohonet: 360 indoor holistic understanding with latent horizontal features. In *Proc. CVPR*, pages 2573–2582, 2021. 1, 2, 3, 6
- [26] Keisuke Tateno, Nassir Navab, and Federico Tombari. Distortion-aware convolutional filters for dense prediction in panoramic images. In *Proc. ECCV*, pages 707–722, 2018. 2, 6
- [27] Weiyue Wang and Ulrich Neumann. Depth-aware cnn for rgbd segmentation. In *Proc. ECCV*, pages 135–150, 2018. 3
- [28] Yajie Xing, Jingbo Wang, and Gang Zeng. Malleable 2.5 d convolution: Learning receptive fields along the depth-axis for rgbd scene parsing. In *Proc. ECCV*, pages 555–571. Springer, 2020. 3
- [29] Mai Xu, Yuhang Song, Jianyi Wang, MingLang Qiao, Liangyu Huo, and Zulin Wang. Predicting head movement in panoramic video: A deep reinforcement learning approach. *IEEE Trans. Pattern Anal. Mach. Intell.*, 41(11):2693–2708, 2018. 1
- [30] Yanyu Xu, Ziheng Zhang, and Shenghua Gao. Spherical dnns and their applications in 360 images and videos. *IEEE Trans. Pattern Anal. Mach. Intell.*, 2021. 1

- [31] Zihui Xue and Radu Marculescu. Dynamic multimodal fusion. In *Proc. CVPR Workshop*, pages 2575–2584, 2023. 5, 6, 7
- [32] Kailun Yang, Xinxin Hu, Hao Chen, Kaite Xiang, Kaiwei Wang, and Rainer Stiefelhagen. Ds-pass: Detail-sensitive panoramic annular semantic segmentation through swaft-net for surrounding sensing. In *Proc. IEEE Intell. Vehicles Symp.*, pages 457–464. IEEE, 2020. 2
- [33] Kailun Yang, Xinxin Hu, and Rainer Stiefelhagen. Is context-aware cnn ready for the surroundings? panoramic semantic segmentation in the wild. *IEEE Trans. Image Process.*, 30:1866–1881, 2021. 1
- [34] Kailun Yang, Jiaming Zhang, Simon Reiß, Xinxin Hu, and Rainer Stiefelhagen. Capturing omni-range context for omnidirectional segmentation. In *Proc. CVPR*, pages 1376–1386, 2021. 1
- [35] Jiaming Zhang, Kailun Yang, Chaoxiang Ma, Simon Reiß, Kunyu Peng, and Rainer Stiefelhagen. Bending reality: Distortion-aware transformers for adapting to panoramic semantic segmentation. In *Proc. CVPR*, pages 16917–16927, 2022. 2, 6
- [36] Jiaming Zhang, Huayao Liu, Kailun Yang, Xinxin Hu, Ruiping Liu, and Rainer Stiefelhagen. Cmx: Cross-modal fusion for rgb-x semantic segmentation with transformers. *IEEE Trans. Intelligent Transportation Systems.*, 24(12):14679–14694, 2023. 3, 6
- [37] Jiaming Zhang, Kailun Yang, Hao Shi, Simon Reiß, Kunyu Peng, Chaoxiang Ma, Haodong Fu, Philip HS Torr, Kaiwei Wang, and Rainer Stiefelhagen. Behind every domain there is a shift: Adapting distortion-aware vision transformers for panoramic semantic segmentation. *IEEE Trans. Pattern Anal. Mach. Intell.*, 46(12):8549–8567, 2024. 2, 6
- [38] Pingping Zhang, Wei Liu, Yinjie Lei, and Huchuan Lu. Hyperfusion-net: Hyper-densely reflective feature fusion for salient object detection. *Pattern Recognition*, 93:521–533, 2019. 3
- [39] Guangcong Zheng, Xianpan Zhou, Xuewei Li, Zhongang Qi, Ying Shan, and Xi Li. Layoutdiffusion: Controllable diffusion model for layout-to-image generation. In *Proc. CVPR*, pages 22490–22499, 2023. 1
- [40] Zishuo Zheng, Chunyu Lin, Lang Nie, Kang Liao, Zhiping Shen, and Yao Zhao. Complementary bi-directional feature compression for indoor 360deg semantic segmentation with self-distillation. In *Proc. WACV*, pages 4501–4510, 2023. 6
- [41] Chuanqing Zhuang, Zhengda Lu, Yiqun Wang, Jun Xiao, and Ying Wang. Acdnet: Adaptively combined dilated convolution for monocular panorama depth estimation. In *Proc. AAAI*, pages 3653–3661, 2022. 2